Reducing Number Fluctuations in an Ultracold Atomic Sample Using Faraday Rotation and Iterative Feedback

R. Thomas[1],[*] J.S. Otto,[2] M. Chilcott,[2] A.B. Deb,[2] and N. Kjærgaard[2],[†]

[1]*Department of Quantum Science and Technology, Research School of Physics, The Australian National University, Canberra 2601, Australia*

[2]*Department of Physics, QSO-Centre for Quantum Science, and Dodd-Walls Centre, University of Otago, Dunedin 9016, New Zealand*

We demonstrate a method to reduce number fluctuations in an ultracold atomic sample using real-time feedback. By measuring the Faraday rotation of an off-resonant probe laser beam with a pair of avalanche photodetectors in a polarimetric setup, we produce a proxy for the number of atoms in the sample. We iteratively remove a fraction of the excess atoms from the sample to converge on a target proxy value in a way that is insensitive to environmental perturbations and robust to errors in light polarization. Using absorption imaging for out-of-loop verification, we demonstrate a reduction in the number fluctuations from 3% to 0.45% for samples at a temperature of 16.4 μK over the time scale of several hours, which is limited by temperature fluctuations, beam-pointing noise, and photon shot noise.

I. INTRODUCTION

The ability to isolate, trap, and cool samples of atoms to ultralow temperatures (approximately 1 μK) has allowed for the exploration of many questions in fundamental quantum science as well as the development of novel sensors with unprecedented precision and accuracy. Ultracold atomic systems have been used to study soliton dynamics [1,2], phase separation [3,4], super- and subradiance [5,6], magnetic order [7], quantum phase transitions [8–10], and fundamental chemistry [11–13]. Ultracold atoms are also the basis of the next generation of optical clocks [14], inertial sensors [15–18], and other metrological devices [19], some of which can take advantage of mesoscopic quantum entanglement to enhance their precision [20,21].

For many of these systems, both the number of atoms in an ultracold sample and the sample density are key parameters that strongly affect their dynamics. For example, in Bose-Einstein condensates, the mean-field energy is determined by the total number of atoms in a condensate and in Fermi gases, the Fermi energy is similarly determined by atom number. In experiments that probe scattering dynamics, the number of atoms scattered per unit time is a function of both the density and the total number of atoms [22–24] and in many other studies, ranging from subradiance [5] to quantum droplets [25,26], the number and/or density of atoms affects phase transitions.

Thus, the precision that can be achieved in such experiments is ultimately dependent on the stability of both the atomic density and number.

The preparation of an ultracold atomic cloud with a fixed number of atoms is a task that remains experimentally challenging due to the inherent complexity of the apparatus, which hybridizes several different technologies from optical, microwave, vacuum, electronic, and mechanical engineering [27,28]. The starting point for an ultracold sample is atoms captured in a magneto-optical trap. These atoms are then typically laser cooled in a sub-Doppler scheme and transferred to a magnetic trap, an optical dipole trap, or a combination of both. There is an inevitable stochastic element to this step and when, finally, this trapped sample is evaporatively cooled to the ultracold domain, atom-number fluctuations on the percent level are to be expected even for an optimized experimental cycle.

In principle, all inputs to an experiment can be made arbitrarily stable, but in the final accounting external magnetic fields will drift, laser powers will have some noise and laboratory temperatures will change [29]. At some point, rather than attempting to stabilize an experimental input (a laser power, for instance) in order to stabilize the output (the number of atoms), it becomes more practical to stabilize the output directly. For this to work, we need methods for nondestructively measuring the number of atoms and removing excess atoms in real time. An early example [30] has shown that frequency-modulation spectroscopy of the scalar light shift [31] provides a non-destructive measurement that can allow for the selection

of experimental cycles where the initial number of atoms is in an acceptable range. Subsequently, Gajdacz *et al.* [32] have used the vector light shift to demonstrate that atomic samples of $N \sim 10^6$ atoms can be produced with fluctuations below the atomic shot noise limit of $\text{Var}(N) = N$. In later works [33,34], the authors have used the same technique to probe number fluctuations in the number of Bose-condensed atoms near the critical temperature. In the latter three experiments, an image of the atomic cloud was taken using dark-field Faraday imaging [35], which allowed the authors to compute a proxy for the number of atoms in the sample. Excess atoms were removed by applying a series of radio-frequency (rf) pulses, each of which removed a small fraction of the remaining atoms. These experiments have all used a far off-resonant laser field to minimize inelastically and off-axis scattered photons and hence heating of the atoms.

While imaging provides a wealth of spatial information, the addition of a camera adds significant complications to real-time data acquisition and processing. Since the total number of atoms in a sample can be related to the integrated signal in the dark-field technique, in principle one can replace the camera with a sufficiently low-noise photodetector. This replacement has three main advantages. First, readout and processing of a voltage signal is both simpler and faster than readout and processing of camera pixel counts. Second, the increased speed at which data can be acquired and processed opens up the possibility of stabilizing the number of atoms by an iterative scheme using multiple stages of measurement and feedback rather than the previously demonstrated single-stage method [32–34]. A multistage method can be less sensitive to changes in the environment and the experimental parameters, making it a potentially more robust stabilization scheme. Multiple stages of feedback can also eliminate the noise floor imposed on the atom number by the stochastic manner in which atoms are removed [32]. Finally, photodetectors are significantly smaller, lighter, and consume less power than a camera, which may be important for mobile or space-based cold-atom devices, where size, weight, and power (SWaP) are important [17,36].

In this paper, we demonstrate a simplified method for stabilizing the number of atoms in an ultracold atomic sample. By combining the polarimetric signals resulting from two probe lasers with different frequencies that interact with the atoms and impinge on two low-noise photodetectors, we obtain a measure of the number of atoms that is insensitive to changes in optical power and photodetector gain. We use the processed signal to inform a multistage feedback protocol that iteratively converges on a target signal, and we demonstrate a reduction in both short and long-term fluctuations in the number of atoms to a relative cycle-to-cycle stability of 0.45%, which is limited by temperature fluctuations, photon shot noise, and beam-pointing fluctuations.

II. IMPLEMENTATION

Generally, feedback to control a system parameter requires three components: a measurement of the parameter of interest, an actuator that affects the parameter, and a controller that can compute the actuator level from the measurement at speeds faster than the fluctuations that one wishes to remove. Our system comprises a prolate sample of ^{87}Rb atoms in the $|F = 2, m_F = 2\rangle$ hyperfine state confined in a Ioffe-Pritchard (IP) magnetic trap with a radial trapping frequency of $\omega_r = 2\pi \times 160$ Hz and a 10:1 aspect ratio. We use Faraday rotation [35,37,38] of off-resonant linearly polarized laser fields propagating along the long axis of the IP trap to generate a signal that is a proxy for the number of atoms in our sample at a fixed temperature.

To describe the effect of Faraday rotation, we start by considering an optical field with wave number k propagating in the z direction. We write the laser polarization after the field has passed through the atoms in terms of the left- and right-circularly polarized components $\hat{\mathbf{e}}_\pm$

$$\mathbf{E} = E_+ e^{i\phi_+} \hat{\mathbf{e}}_+ + E_- e^{i\phi_-} \hat{\mathbf{e}}_-, \tag{1}$$

with amplitudes $E_\pm$ and phases $\phi_\pm$ that, in general, are functions of the coordinates transverse to the direction of propagation of the light (x, y). Faraday rotation in atomic systems is caused by a difference in the electric susceptibility for the right- and left-circularly polarized components due to differences in the transition dipole-matrix elements. If the detuning of the field from resonance, Δ, is much larger than the natural line width of the optical transition, Γ, we can neglect absorption of the field and write the phase shifts imparted by a gas of transverse density $\rho(x, y)$ as

$$\phi_\pm(x, y) = \left(\frac{k}{2\epsilon_0 \hbar} \sum_b \frac{|d_{ab}|^2}{\Delta + \Delta_b} \right) \rho(x, y) = \xi_\pm \rho(x, y), \tag{2}$$

where d_{ab} is the dipole-matrix element connecting ground state a to excited state b and Δ_b is the additional detuning associated with excited state b due, for instance, to hyperfine splitting of the excited-state levels. Equations (1) and (2) are valid in the regime where we collect all light in the incident and scattered fields and where we can neglect diffraction of light during propagation through the sample [39]. We use a dual-port measurement scheme as presented in Fig. 1 for measuring the rotation angle. Defining

$$r_0 = \frac{2|E_+||E_-|}{|E_+|^2 + |E_-|^2} \tag{3}$$

as the degree of linear polarization, the power in the x (horizontal) and y (vertical) polarization components is

$$P_x = \frac{P}{2} \left[1 + r_0 s_a \cos\alpha + r_0 c_a \sin\alpha \right], \tag{4a}$$

$$P_y = \frac{P}{2}\left[1 - r_0 s_a \cos\alpha - r_0 c_a \sin\alpha\right], \qquad (4b)$$

with total optical power P, and

$$s_a = \frac{2}{\pi w^2}\int e^{-2(x^2+y^2)/w^2}\sin\phi_a(x,y)dxdy, \qquad (5a)$$

$$c_a = \frac{2}{\pi w^2}\int e^{-2(x^2+y^2)/w^2}\cos\phi_a(x,y)dxdy, \qquad (5b)$$

with Gaussian beam waist w and $\phi_+ - \phi_- = \pi/2 + \alpha + \phi_a$. Here, $\phi_a(x,y) = (\xi_+ - \xi_-)\rho(x,y) = \xi\rho(x,y)$ is the differential phase shift solely due to the atomic sample and $\pi/2 + \alpha$ is the differential phase shift from all other sources. With these definitions of r_0 and α, linearly polarized light at $45°$ has $r_0 = 1$ and $\alpha = 0$. We convert the optical power into voltages using two avalanche photodetectors (APDs) and then digitize the results using the two analog-to-digital convertors (ADCs) on a Red Pitaya (RP) STEMlab 125-14 development board to produce signals S_x and S_y, which are linearly related to the optical powers P_x and P_y via $S_x = g_x P_x$ and $S_y = g_y P_y$. The gains g_x and g_y include the APD gains, the ADC conversion gains, and any inefficiencies in coupling the light onto the photodetectors.

If the gains g_x and g_y are known, then one can form linear combinations of the x and y signals, $\mathcal{S}_\pm = g_y S_x \pm g_x S_y$, and the ratio $\mathcal{R} = \mathcal{S}_-/\mathcal{S}_+$ depends only on the light polarization and the atomic phase shift:

$$\mathcal{R} = r_0\left(s_a \cos\alpha + c_a \sin\alpha\right). \qquad (6)$$

However, small errors in the gain coefficients used in cross multiplication will lead to small offsets in $\mathcal{R}$ which, if time dependent, will degrade the precision of the inferred atom-number proxy. We use temperature-compensated APDs (Thorlabs APD430A), which have gain stabilities on the order of 1% at ambient temperatures. Additionally, our laser field propagates along a 2-m path and although we use lenses to focus the laser onto the APDs, beam-pointing instabilities still lead to changes in the optical power that reaches the detectors, which mimic changes in the photodetector gains. Together, these changes can lead to variations on the order of several percent in our Faraday signal, which, if applied in a feedback loop, ultimately limits the atom-number stability to the same level.

Fluctuations in the laser power, laser pointing, and photodetector gains can be circumvented by using two laser frequencies in a differential measurement. As shown in Fig. 1, we combine two laser fields L and L' using a fiber beam splitter and interleave pulses from the two lasers. As long as the time between pulses from L and L' is much shorter than the typical time scale for variations in photodetector gain and beam-pointing fluctuations, we can assume that the effective gains for each laser field are the same. By choosing the frequencies of L and L' to be on opposite sides of the resonance, the difference in phase shifts from the two fields leads to an enhanced signal. We combine the signals from lasers L and L' to form the ratio

$$R = \frac{S_x S_y' - S_x' S_y}{S_x S_y' + S_x' S_y}, \qquad (7)$$

which can be expressed in terms of the physical system as

$$R = \frac{r_0\left[(s_a - s_a')\cos\alpha + (c_a - c_a')\sin\alpha\right]}{1 - r_0^2(c_a\sin\alpha + s_a\cos\alpha)(c_a'\sin\alpha + s_a'\cos\alpha)}, \qquad (8)$$

where s_a' and c_a' are the weighted atomic phase differences for laser L' and we assume that the polarizations of L and L' are the same. R is insensitive to changes in the optical powers of either L or L', drift in the gains of the photodetectors, and, by sharing a common path and spatial mode, R is also insensitive to small changes in the beam alignment onto the APDs. If we have a Gaussian density profile with N atoms and spatial standard deviation $\kappa = \sqrt{k_B T/m\omega_r^2}$ with temperature T and mass m and we operate in a regime where the phase shifts are small, corresponding to large laser detunings and/or low-density atomic samples, R can be approximated as

$$R \approx \frac{2(\xi - \xi')N}{\pi(w^2 + 4\kappa^2)}r_0\cos\alpha - \frac{(\xi^2 - \xi'^2)N^2}{4\pi^2\kappa^2(w^2 + 2\kappa^2)}r_0\sin\alpha. \qquad (9)$$

Ideally, $\alpha = 0$ and $r_0 = 1$, corresponding to linearly polarized light at $45°$, although small deviations from these values only lead to either a reduced signal strength or a weak second-order dependence on the peak differential phase shift. We set the polarization at the final polarizing beam splitter in the absence of atoms by first adjusting the last two wave plates to minimize the amount of light on one APD and then setting the final half-wave plate such that output of the APD is half of its maximum value. This method allows us to compensate for any birefringence in the vacuum windows or the dielectric coated optics, as polarization changes that occur after the atoms can always be reversed. An important feature of our technique is that the performance of feedback is insensitive to small errors in the polarization as long as those errors are independent of time, since the computation of R from measurements makes no assumption about the polarization of the light.

As seen in Eq. (9), the waist of the laser field is an important parameter for feedback. When the waist is much smaller than the size of the sample, R is a sensitive probe of the central density of the sample and attains its maximum signal strength. When $w \gg \kappa$, however, R measures the atom number N directly with minimal dependence on sample size but with a reduced signal strength. Our probe beam waist of $w \approx 60\ \mu$m is approximately the same as
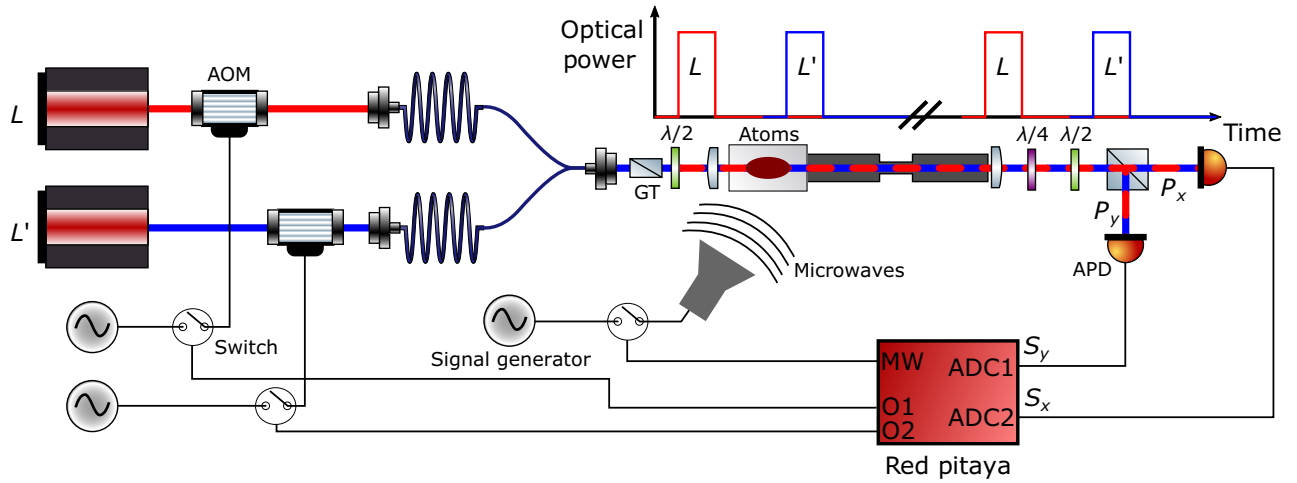
FIG. 1.   A simplified diagram of the experiment. Two lasers, routed through two acousto-optic modulators (AOMs), are combined using a fiber beam combiner. The polarization of the two lasers is set by a Glan-Thompson prism (GT) and then rotated to the desired polarization with a half-wave plate. The combined fields are focused onto the atoms in the science cell using a lens and the light is collected by another lens after the light has propagated through approximately 1 m of vacuum system, including an aperture between high- and ultrahigh-vacuum sections. A quarter- and half-wave plate correct the polarization and set it to $+45°$ before the light passes through a polarizing beam-splitting cube. The two polarization components impinge on two avalanche photodetectors (APDs) and the two voltage signals are digitized using a Red Pitaya (RP) development board, which controls the light pulses and the microwave state.

the radial size of the atomic sample at the temperature we investigate as a compromise between signal-to-noise ratio and our ability to collect the light at the far end of our vacuum system.

One of our laser fields is sourced from a laser that is offset locked -3 GHz from the ^{87}Rb $F = 2 \to F' = 3$ transition (L) and the other field is sourced from our magneto-optical trap (MOT) repump laser, which is locked to the $F = 1 \to F' = 2$ transition (L'). The power incident on the uncoated glass surface of our vacuum window is 2.5 μW for laser L and 5.0 μW for laser L'. If we assume 4% loss of optical power per surface from Fresnel reflection, we can expect to pump atoms to other hyperfine states at a fractional rate of 4.8×10^{-5} μs^{-1} and to heat the sample at a rate of 24 pKμs^{-1}. These rates should be interpreted as upper limits, as we measure a 35% loss of optical power through the entire vacuum system comprising four glass surfaces and the distribution of this loss across the four windows is unknown. We lose an additional 39% of optical power between the exit vacuum window and the APDs, for a total loss of 60%. Figure 2 shows how the measured value of R changes when the number of atoms at a fixed trap depth as measured by absorption imaging is varied by changing the number of atoms loaded into our IP trap. Due to changes in evaporative cooling efficiency and thermalization rates with the number of atoms loaded into the IP trap, the temperature of the sample varies with the number of atoms from 29 μK for the lowest number of atoms to 16.2 μK for the highest number of atoms. We obtain good agreement with the theoretical prediction of

Eq. (8) if we multiply the measured number of atoms by 1.073, indicating that our absorption images undercount the number of atoms. A systematic error of this size can arise from a number of different sources related to absorption imaging, such as errors in calibrating the magnetic field direction during imaging, effective camera gain, or image magnification, with the most likely cause being an error in calibrating the magnetic field direction, as we use an ambient field to define our quantization axis relative to the imaging light polarization. An accounting of the statistical uncertainty in absorption imaging is provided later in the paper.

For our actuator, we use microwave pulses resonant with the $|2, 2\rangle \to |1, 1\rangle$ transition at approximately 6.8 GHz. We follow previous work [32,33] and use many short pulses to remove atoms from the sample by transferring small fractions to the antitrapped $|1, 1\rangle$ state where atoms are expelled from the trap. We use 25-μs-long pulses, each of which transfers approximately $f \approx 10^{-3}$ of the atoms in the $|2, 2\rangle$ state to the $|1, 1\rangle$ state, and the microwave pulses are spaced by 50 μs. For sufficiently small transfer fraction per pulse, we can approximate the number of pulses needed to remove a given fraction of atoms as a linear function of f^{-1}. This choice of many short pulses, as opposed to a single longer pulse, simplifies the calculation of the actuator value and avoids transferring a large fraction of atoms to the $|1, 1\rangle$ state, where the L' laser is close to resonance and thus would be more strongly affected by the antitrapped atoms than the trapped atoms. As our sample is magnetically trapped and the natural line width
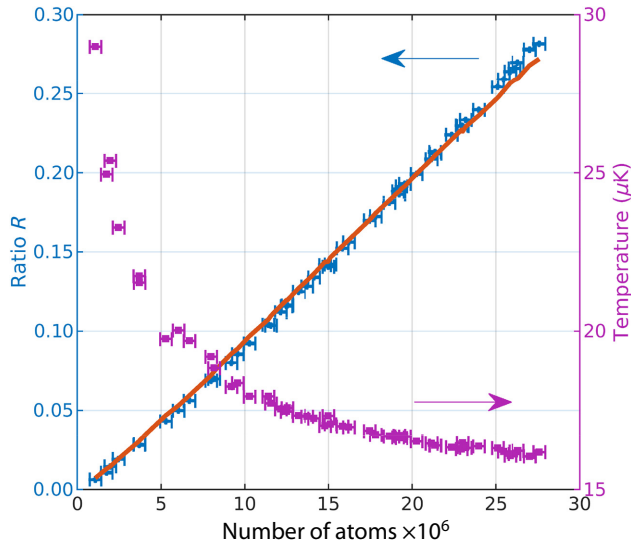
FIG. 2. The measured value of R (blue circles, left axis) and the sample temperature (purple squares, right axis) as a function of the number of atoms N at a detuning of -3 GHz for L and 6.8 GHz for L'. Due to the manner in which the number of atoms is changed, the temperature of the sample also changes. The solid red line is the prediction from Eq. (8) with N scaled by 1.073.

FIG. 3. The effect of microwave pulses on a sample of atoms at an initial temperature of 16 μK for 1000 microwave pulses that are 25 μs wide and spaced by 50 μs. Detuning is relative to the microwave frequency at zero magnetic field. The left axis (blue circles) shows the remaining number of atoms while the right axis (red squares) shows the change in the temperature as a function of the microwave frequency. The gray dashed line shows the approximate microwave frequency at which the change in temperature is zero.

of the microwave transition is negligible, the microwave field only addresses atoms in a narrow energy range, the width of which is defined by the temporal width and Rabi frequency of the pulse. Therefore, the number of atoms removed as a function of the microwave frequency will reflect the potential energy distribution of the atoms, as shown in Fig. 3. An important consequence of this energy selectivity is that the microwave pulses will heat (cool) the sample when the microwave frequency is set too low (high). Theoretically, the microwave frequency should be set to be resonant with the mean energy of the sample [33]; in practice, we experimentally determine the optimum frequency by measuring the change in temperature of the sample as a function of the microwave frequency as in Fig. 3.

To unite our measurement with our actuator and close the feedback loop, we use programmable logic on a 14-bit RP development board. Our feedback protocol proceeds as follows. First, the RP pulses on L then L' for a programmable duration with the L' pulse delayed relative to the L pulse and the resulting APD voltages are captured by the two ADCs on the RP. The signal values $S_{x,y}$ and $S'_{x,y}$ are calculated as the difference between the mean APD voltages when the pulses are on and when the pulses are off, to account for any offset voltages on the ADCs. The ratio R_{j-1} is then calculated from the integrated signals as in Eq. (7) to 16 bits of precision. R_{j-1} is compared with a target value, R_{target}, and we calculate the number of microwave pulses n_j to apply for the current feedback
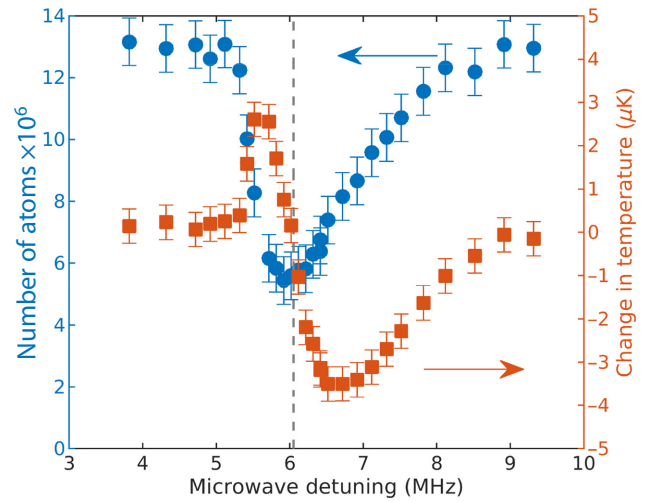
round j as

$$n_j = \left\lfloor bf^{-1}\left(\frac{R_{j-1} - R_{target}}{R_{j-1}}\right)\right\rfloor, \qquad (10)$$

where b is the fraction of excess atoms to remove in a given round j and R_0 is the initial value of R. After j rounds of feedback, the measured ratio will be

$$R_j = R_{target} + (R_0 - R_{target})(1 - b)^j. \qquad (11)$$

The feedback protocol described by Ref. [32] effectively implements Eq. (11) with $b = 1$, where all the excess atoms are removed after a single measurement. If, however, the fraction of atoms removed with each microwave pulse changes or is not well known, then a single round of feedback will not necessarily produce a sample with the target number of atoms. Additionally, the stochastic nature of removing atoms leads to an uncertainty in the final number of atoms that increases with the number of atoms removed [32,40]. Both of these effects result in the final fluctuations in the number of atoms depending on the number of atoms removed relative to the target value in the last feedback round. Therefore, we use $b = 0.25$ to $b = 0.5$ and we terminate feedback when $R_j < (1 + tol)R_{target}$, where tol is a fractional tolerance value that we set to 1×10^{-3}. Example decay curves of R are shown in Fig. 4 for $b \approx 0.4$, corresponding to $f \approx 1.5 \times 10^{-3}$, and $R_{target} = 0.24$. The
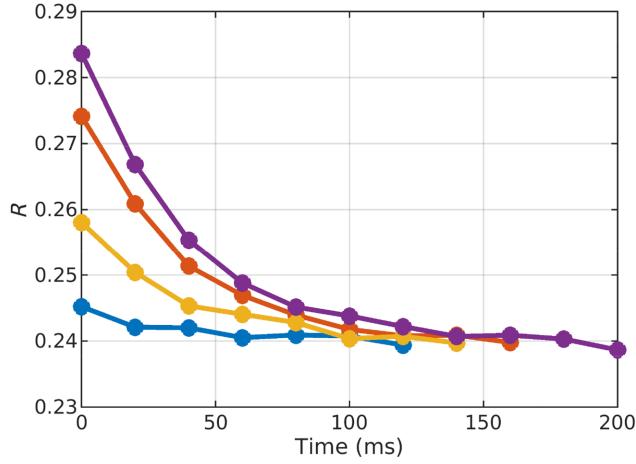
FIG. 4. Example data showing the decay of the value of R during feedback. Each set is a different run of the experiment with different initial numbers of atoms at fixed temperatures. The target value is set to $R_{\mathrm{target}} = 0.24$ with a tolerance of 10^{-3}. The value of b for these curves is $b \approx 0.4$.

number of atoms to remove in the last round relative to the target is then bounded from above by

$$\frac{R_{j-1} - R_{\mathrm{target}}}{R_{\mathrm{target}}} \leq \frac{\mathrm{tol}}{1-b}, \tag{12}$$

which is 1.7×10^{-3} for the parameters given above. Relative fluctuations in the final number of atoms caused by relative fluctuations in f are further reduced by a factor of b, resulting in a suppression factor of 6.7×10^{-4}. Fluctuations in the final number caused by the stochastic removal of atoms are reduced below the shot noise level by the square root of this factor, or 2.6×10^{-2}, regardless of the initial number of atoms.

III. RESULTS

Figure 5 shows the effect of our iterative feedback scheme on a sample of ^{87}Rb atoms held in our IP trap at a temperature of 16.3 μK, where we set $R_{\mathrm{target}} = 0.24$ corresponding to $N_{\mathrm{target}} = 25.7 \times 10^6$ atoms. Each round of feedback comprises a measurement of R using pulses from L and L' that are 50 μs long with the pulses from L' delayed by 1.5 ms, followed by application of a variable number of microwave pulses. Each pair of pulses, which define the start of a feedback round, are separated in time by 20 ms, this being chosen to allow enough time for all possible microwave pulses to be applied. The number of microwave pulses is calculated by the RP using Eq. (10), with $bf^{-1} = 250$ defining the maximum number of microwave pulses that can be applied. The exact value for the maximum number of microwave pulses is unimportant, except that a larger value leads to fewer feedback rounds at the cost of greater sensitivity to fluctuations in f.

We measure the number of atoms and the temperature at the end of a cycle using standard absorption imaging resonant with the $F = 2 \to F' = 3$ transition along one of the radial axes after releasing the atoms from the IP trap and waiting for 15 ms. This serves as an important independent measure of the number of atoms, as feedback in general suppresses fluctuations in the measurement (R) but not necessarily in the system state (N) [41]. Our absorption imaging light is turned on for 250 μs at an intensity of 67 μW cm^{-2}. The quantum efficiency of the camera sensor at our imaging wavelength is 0.8 and the photon shot noise dominates over the readout noise with our effective pixel size of 11 μm $\times$ 11 μm. From these parameters, we attribute relative fluctuations on the number of atoms of 0.014% from photon shot noise. A much larger contribution comes from inhomogeneity in the imaging fields, such as fringes caused by the relatively long separation between pairs of images of 18 ms, which we estimate from Monte Carlo simulations of the fitting process and images to be 0.4%.

The data in Fig. 5 comprise 425 experimental cycles over the course of 10 h, where we randomly choose to enable or disable feedback with 50% probability. When feedback is disabled, we do not apply any optical pulses in order to measure the free-running distribution of atom numbers and temperatures. As can be seen in Figs. 5(a)–5(d), our experiment shows significant cycle-to-cycle variations in the number of atoms in addition to long-term drift over the course of a day, while the temperature remains nearly constant. We set R_{target} such that the desired number of atoms is close to the initial number of atoms at the start of the day. Early in the series, feedback engages sporadically as $R_0 < R_{\mathrm{target}}$; however, these cases are easily detected in postprocessing, as only one feedback round is attempted. As a result, in experiments where the free-running number of atoms shows no drift, the number can be stabilized to the mean free-running value with only a 50% reduction in the experimental duty cycle. This will be advantageous when the variance in the free-running number of atoms is more than twice the variance in the stabilized number of atoms, as the decreased variance will more than compensate for the increased cycle time.

In the latter half of the time series of Fig. 5, the free-running number of atoms almost always exceeds the target value and thus feedback is almost always applied. The result is that the cycle-to-cycle fluctuations and the drift in the number of atoms are significantly reduced. Figures 5(c) and 5(d) show that the temperature of the sample under feedback tends to be slightly lower than the temperature absent feedback. This change in temperature is caused by setting the microwave frequency slightly too high relative to the mean energy of the atoms. The change in temperature is equivalent to approximately -2 nK/pulse and this change is noticeable in the latter part of the time series because more microwave pulses are required to
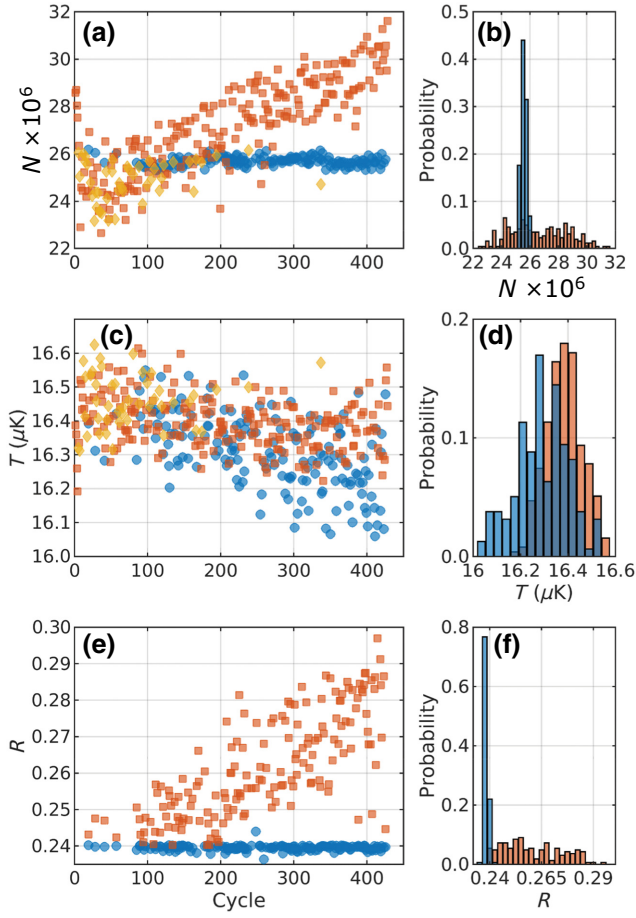
FIG. 5. The effect of feedback on a sample of atoms. The red squares and bars indicate cycles when feedback is disabled, blue circles and bars indicate when feedback is applied, and yellow diamonds indicate when feedback is enabled but $R_0 < R_{target}$ and feedback is not applied. (a),(b) The number of atoms in the sample as measured by absorption imaging. (c),(d) The temperature of the sample. (e),(f) The initial and final values of R when feedback is applied. The blue circles and bars indicate the final value of R and the red squares and bars indicate the initial value R_0.

remove enough atoms to reach the target value. This effect dominates over the expected heating rate from the optical pulses, which is approximately 1.3 nK per feedback round.

To quantify the variation in the number of atoms, we use the overlapped estimator of the Allan variance [42],

$$\sigma_x^2(\tau) = \frac{1}{2(M - 2\tau)\tau^2}$$

$$\times \sum_{k=0}^{M-2\tau-1} \left[\sum_{j=\tau+k}^{2\tau+k-1} x_j - \sum_{j=k}^{\tau+k-1} x_j \right]^2, \quad (13)$$

where M is the number of samples in a data set $\{x_j\}$ and τ is the offset at which to calculate the Allan variance $\sigma^2(\tau)$. We plot the relative Allan deviation $\sqrt{\sigma_x^2(\tau)}/\langle x \rangle$

in Fig. 6 for the number of atoms measured with and without feedback (filled markers), labeled N_{free} and N_{stab}, respectively, and the initial (R_0) and final (R_f) values of R when feedback is applied (open markers). The cycle-to-cycle variations of N_{free} and R_0 when feedback is disabled are about 3.5% and both show significant drift over the course of a day. In contrast, the cycle-to-cycle variations in the controlled values of N_{stab} and R_f show relative fluctuations of 0.65% and 0.32%, respectively. To assess the "true" performance of our method, we estimate the number of atoms from R_f and our measurements of the temperature T using Eq. (9) and we plot the relative Allan deviation of this quantity as N_{est} in Fig. 6 as the solid green line. The cycle-to-cycle variations in N_{est} amount to 0.45% and when added in quadrature with the estimated uncertainty from absorption imaging, agree well with the short-term measured variations in N_{stab} as seen by the dashed green line in Fig. 6. In the longer term, there is more variation in N_{stab} than in N_{est}, which is likely due to changes in the calibration between the true number of atoms and the number of atoms measured by absorption imaging. While a number of different factors that contribute to the absorption imaging calibration may vary with time, in our experiment the most likely candidate is a change in the imaging magnetic field strength and direction. For long averaging times, N_{est} starts to show some drift, as evidenced by the upward trajectory of the relative Allan deviation in Fig. 6. This is caused by the change in temperature when feedback is enabled, as seen in Fig. 5(c), and could be reduced by a more careful calibration of the microwave frequency or use of a larger probe beam size at the expense of a lower signal-to-noise ratio.

Our cycle-to-cycle fluctuations in R limit the final stability of the atom number, since feedback cannot stabilize a parameter to a higher precision than to which one can measure that parameter. Based on our applied laser powers and pulse durations as well as the noise-equivalent powers of our detectors (140 pWHz$^{-1/2}$) and the noise floor of the ADCs of the RP (50 nVHz$^{-1/2}$), our measurement is dominated by photon shot noise [43] and this imposes a limit on the cycle-to-cycle stability of 0.15%. Stochastic loss of atoms to other hyperfine states due to optical pumping can lead to additional noise [40] but we have estimated this to contribute relative fluctuations of only 2×10^{-5} based on the aforementioned loss rates and pulse durations. Additional pulses applied after feedback has terminated confirm that our final stability is due to fluctuations from pulse to pulse, not from cycle to cycle. We attribute the excess noise on our measurement of R to beam-pointing noise arising from two different processes. First, beam-pointing noise onto the atoms causes changes in R as the overlap between the sample and the laser fields changes. Second, the sample acts as a lens [39] with different focal lengths for the different circular polarization components and a small change in the beam position on the atoms maps to different final beam
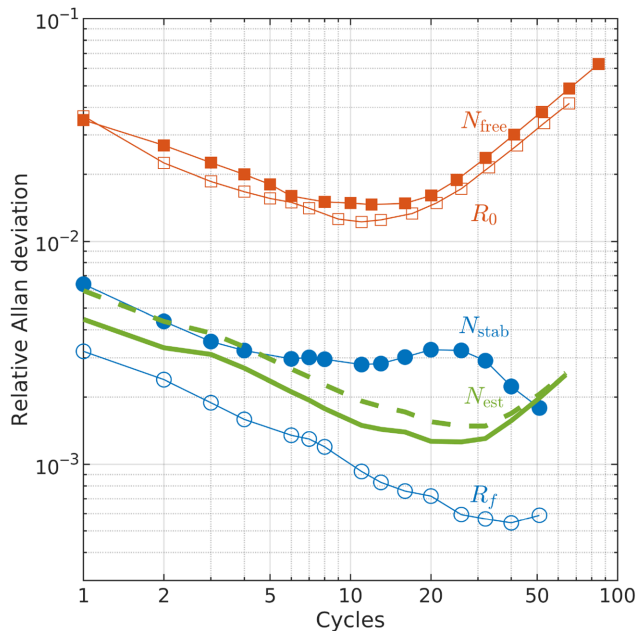
FIG. 6. The relative Allan deviations of the number of atoms N and the ratio R. The Allan deviations for the number of atoms are indicated by filled markers, where blue circles are the Allan deviation with feedback applied (N_{stab}) and the red squares are without feedback (N_{free}). The Allan deviations for R when feedback is applied are indicated by open markers, where the blue circles are for the final value of R when feedback terminates (R_f) and the red squares are the Allan deviation for initial values (R_0). The solid green line is the relative Allan deviation from the estimated number of atoms N_{est} from R_f, the measured temperature, and Eq. (9), and the dashed green line is the sum in quadrature of the Allan deviation of N_{est} and the estimated imaging noise.

positions for the different polarizations. Effectively, this leads to pulse-to-pulse changes in r_0 and hence R. Reduction of the beam-pointing noise would require significant redesign of our apparatus but other apparatuses need not suffer the same problem and may be able to reach the limit imposed by photon shot noise.

IV. CONCLUSION

In this paper, we demonstrate a simple method for reducing the fluctuations in the number of atoms in an ultracold sample. We use a differential measurement of the off-resonant Faraday rotation of two laser fields as they propagate through the sample to compute a proxy for the number of atoms that is independent of changes in laser power and photodetector gain and is only weakly sensitive to alignment. For sufficiently large detunings, this proxy value is linear in the number of atoms for a fixed temperature. By using an iterative feedback scheme, we reduce the need for precalibration of our control system, which makes it more robust to environmental perturbations. We independently measure fluctuations in the number of atoms using

absorption imaging and we demonstrate a reduction in the cycle-to-cycle number fluctuations down to 0.45%, which is limited by temperature fluctuations, photon shot noise, and beam-pointing noise.

Apparatuses with better optical design will likely be able to eliminate beam pointing as a source of noise, leaving temperature fluctuations and photon shot noise as the leading contributions. Sensitivity to temperature changes can be reduced by using a beam size that is larger than the size of the sample, at a cost of a reduced signal-to-noise ratio. Alternatively, feedback could be applied to atoms trapped in an optical dipole trap, where microwave fields are resonant with the entire sample and trapping parameters are more easily controlled, although the actuator would then require a dissipative element such as a resonant optical field. If we suppose that these two sources of noise can be eliminated, the effect of photon shot noise can be strongly reduced by using higher optical powers and/or longer pulse durations. A straightforward calculation shows that with the incident optical powers used in this study, one can stabilize 26×10^6 atoms to a factor of 2 below the atomic shot-noise level with pulses that are 4 ms long [40]. A two-step feedback method [32], where one removes most of the atoms in the first step and then removes only a small fraction in the second step, may be required in this situation to minimize heating of the sample and loss to other hyperfine states.

Although our reported cycle-to-cycle fluctuations in our feedback measurement are a factor of approximately 5 larger than the state of the art [32,33], our control system has a number of advantages. It is both simpler and less costly in terms of equipment and data processing and it is also faster, which allows for an iterative scheme to be used that is more robust to calibration errors. In applications requiring portable atom-based devices, our system has significant advantages in terms of SWaP. Finally, by using microwave pulses instead of rf pulses, our method is easily adapted to feedback control of the number of atoms in dual-species experiments.

During preparation of this paper, we have become aware of recent related work using an optical cavity for dispersive real-time tracking of evaporative cooling with cavity-assisted feedback stabilization of atom number as a future goal [44].

[1] S. Burger, K. Bongs, S. Dettmer, W. Ertmer, K. Sengstock, A. Sanpera, G. V. Shlyapnikov, and M. Lewenstein, Dark Solitons in Bose-Einstein Condensates, Phys. Rev. Lett. **83,** 5198 (1999).

[2] P. J. Everitt, M. A. Sooriyabandara, M. Guasoni, P. B. Wigley, C. H. Wei, G. D. McDonald, K. S. Hardman, P. Manju, J. D. Close, C. C. N. Kuhn, S. S. Szigeti, Y. S. Kivshar, and N. P. Robins, Observation of a modulational instability in Bose-Einstein condensates, Phys. Rev. A **96,** 041601(R) (2017).

[3] S. B. Papp, J. M. Pino, and C. E. Wieman, Tunable Miscibility in a Dual-Species Bose-Einstein Condensate, Phys. Rev. Lett. **101,** 040402 (2008).

[4] S. Ospelkaus, C. Ospelkaus, L. Humbert, K. Sengstock, and K. Bongs, Tuning of Heteronuclear Interactions in a Degenerate Fermi-Bose Mixture, Phys. Rev. Lett. **97,** 120403 (2006).

[5] G. Ferioli, A. Glicenstein, L. Henriet, I. Ferrier-Barbut, and A. Browaeys, Storage and Release of Subradiant Excitations in a Dense Atomic Cloud, Phys. Rev. X **11,** 021031 (2021).

[6] S. Inouye, A. P. Chikkatur, D. M. Stamper-Kurn, J. Stenger, D. E. Pritchard, and W. Ketterle, Superradiant Rayleigh scattering from a Bose-Einstein condensate, Science **285,** 571 (1999).

[7] L. E. Sadler, J. M. Higbie, S. R. Leslie, M. Vengalattore, and D. M. Stamper-Kurn, Spontaneous symmetry breaking in a quenched ferromagnetic spinor Bose-Einstein condensate, Nature **443,** 312 (2006).

[8] X.-Y. Luo, Y.-Q. Zou, L.-N. Wu, Q. Liu, M.-F. Han, M. K. Tey, and L. You, Deterministic entanglement generation from driving through quantum phase transitions, Science **355,** 620 (2017).

[9] K. Baumann, C. Guerlin, F. Brennecke, and T. Esslinger, Dicke quantum phase transition with a superfluid gas in an optical cavity, Nature **464,** 1301 (2010).

[10] M. Greiner, O. Mandel, T. Esslinger, T. W. Hänsch, and I. Bloch, Quantum phase transition from a superfluid to a Mott insulator in a gas of ultracold atoms, Nature **415,** 39 (2002).

[11] S. Ospelkaus, K.-K. Ni, D. Wang, M. H. G. de Miranda, B. Neyenhuis, G. Quéméner, P. S. Julienne, J. L. Bohn, D. S. Jin, and J. Ye, Quantum-state controlled chemical reactions of ultracold potassium-rubidium molecules, Science **327,** 853 (2010).

[12] J. F. E. Croft, C. Makrides, M. Li, A. Petrov, B. K. Kendrick, N. Balakrishnan, and S. Kotochigova, Universality and chaoticity in ultracold K + KRb chemical reactions, Nat. Commun. **8,** 15897 (2017).

[13] M.-G. Hu, R. S. Bloom, D. S. Jin, and J. M. Goldwin, Avalanche-mechanism loss at an atom-molecule Efimov resonance, Phys. Rev. A **90,** 013619 (2014).

[14] A. D. Ludlow, M. M. Boyd, J. Ye, E. Peik, and P. O. Schmidt, Optical atomic clocks, Rev. Mod. Phys. **87,** 637 (2015).

[15] X. Wu, Z. Pagel, B. S. Malek, T. H. Nguyen, F. Zi, D. S. Scheirer, and H. Müller, Gravity surveys using a mobile atom interferometer, Sci. Adv. **5,** eaax0800 (2019).

[16] K. Hardman, P. Everitt, G. McDonald, P. Manju, P. Wigley, M. Sooriyabandara, C. Kuhn, J. Debs, J. Close, and N. Robins, Simultaneous Precision Gravimetry and Magnetic Gradiometry with a Bose-Einstein Condensate: A High Precision, Quantum Sensor, Phys. Rev. Lett. **117,** 138501 (2016).

[17] C. Freier, M. Hauth, V. Schkolnik, B. Leykauf, M. Schilling, H. Wziontek, H.-G. Scherneck, J. Müller, and A. Peters, Mobile quantum gravity sensor with unprecedented stability, J. Phys. Conf. Ser. **723,** 012050 (2016).

[18] V. Ménoret, P. Vermeulen, N. Le Moigne, S. Bonvalot, P. Bouyer, A. Landragin, and B. Desruelle, Gravity measurements below 10^{-9} g with a transportable absolute quantum gravimeter, Sci. Rep. **8,** 12300 (2018).

[19] L. Pezzè, A. Smerzi, M. K. Oberthaler, R. Schmied, and P. Treutlein, Quantum metrology with nonclassical states of atomic ensembles, Rev. Mod. Phys. **90,** 035005 (2018).

[20] K. C. Cox, G. P. Greve, J. M. Weiner, and J. K. Thompson, Deterministic Squeezed States with Collective Measurements and Feedback, Phys. Rev. Lett. **116,** 093602 (2016).

[21] R. Kohlhaas, A. Bertoldi, E. Cantin, A. Aspect, A. Landragin, and P. Bouyer, Phase Locking a Clock Oscillator to a Coherent Atomic Ensemble, Phys. Rev. X **5,** 021011 (2015).

[22] M. S. J. Horvath, R. Thomas, E. Tiesinga, A. B. Deb, and N. Kjærgaard, Above-threshold scattering about a feshbach resonance for ultracold atoms in an optical collider, Nat. Commun. **8,** 452 (2017).

[23] R. Thomas, K. O. Roberts, E. Tiesinga, A. C. J. Wade, P. B. Blakie, A. B. Deb, and N. Kjærgaard, Multiple scattering dynamics of fermions at an isolated p-wave resonance, Nat. Commun. **7,** 12069 (2016).

[24] R. Thomas, M. Chilcott, E. Tiesinga, A. B. Deb, and N. Kjærgaard, Observation of bound state self-interaction in a nano-eV atom collider, Nat. Commun. **9,** 4895 (2018).

[25] T. Koch, T. Lahaye, J. Metz, B. Fröhlich, A. Griesmaier, and T. Pfau, Stabilization of a purely dipolar quantum gas against collapse, Nat. Phys. **4,** 218 (2008).

[26] L. Chomaz, D. Petter, P. Ilzhöfer, G. Natale, A. Trautmann, C. Politi, G. Durastante, R. van Bijnen, A. Patscheider, M. Sohmen, M. Mark, and F. Ferlaino, Long-Lived and Transient Supersolid Behaviors in Dipolar Quantum Gases, Phys. Rev. X **9,** 021012 (2019).

[27] H. J. Lewandowski, D. M. Harber, D. L. Whitaker, and E. A. Cornell, Simplified system for creating a Bose-Einstein condensate, J. Low Temp. Phys. **132,** 309 (2003).

[28] E. W. Streed, A. P. Chikkatur, T. L. Gustavson, M. Boyd, Y. Torii, D. Schneble, G. K. Campbell, D. E. Pritchard, and W. Ketterle, Large atom number Bose-Einstein condensate machines, Rev. Sci. Instrum. **77,** 023106 (2006).

[29] M. Chilcott and N. Kjærgaard, Low-cost wireless condition monitoring system for an ultracold atom machine, Internet of Things **13,** 100345 (2021).

[30] B. J. Sawyer, A. B. Deb, T. McKellar, and N. Kjærgaard, Reducing number fluctuations of ultracold atomic gases via dispersive interrogation, Phys. Rev. A **86,** 065401 (2012).

[31] J. E. Lye, J. J. Hope, and J. D. Close, Nondestructive dynamic detectors for Bose-Einstein condensates, Phys. Rev. A **67,** 043609 (2003).

[32] M. Gajdacz, A. J. Hilliard, M. A. Kristensen, P. L. Pedersen, C. Klempt, J. J. Arlt, and J. F. Sherson, Preparation of Ultracold Atom Clouds at the Shot Noise Level, Phys. Rev. Lett. **117**, 073604 (2016).

[33] M. A. Kristensen, M. B. Christensen, M. Gajdacz, M. Iglicki, K. Pawłowski, C. Klempt, J. F. Sherson, K. Rzążewski, A. J. Hilliard, and J. J. Arlt, Observation of Atom Number Fluctuations in a Bose-Einstein Condensate, Phys. Rev. Lett. **122**, 163601 (2019).

[34] M. B. Christensen, T. Vibel, A. J. Hilliard, M. B. Kruk, K. Pawłowski, D. Hryniuk, K. Rzążewski, M. A. Kristensen, and J. J. Arlt, Observation of Microcanonical Atom Number Fluctuations in a Bose-Einstein Condensate, Phys. Rev. Lett. **126**, 153601 (2021).

[35] M. Gajdacz, P. L. Pedersen, T. Mørch, A. J. Hilliard, J. Arlt, and J. F. Sherson, Non-destructive Faraday imaging of dynamically controlled ultracold atoms, Rev. Sci. Instrum. **84**, 083105 (2013).

[36] D. C. Aveline, J. R. Williams, E. R. Elliott, C. Dutenhoffer, J. R. Kellogg, J. M. Kohel, N. E. Lay, K. Oudrhiri, R. F. Shotwell, N. Yu, and R. J. Thompson, Observation of Bose-Einstein condensates in an earth-orbiting research lab, Nature **582**, 193 (2020).

[37] B. Julsgaard, A. Kozhekin, and E. S. Polzik, Experimental long-lived entanglement of two macroscopic objects, Nature **413**, 400 (2001).

[38] F. Kaminski, N. S. Kampel, M. P. H. Steenstrup, A. Griesmaier, E. S. Polzik, and J. H. Müller, In-situ dual-port polarization contrast imaging of Faraday rotation in a high optical depth ultracold ^{87}Rb atomic ensemble, Eur. Phys. J. D **66**, 227 (2012).

[39] A. B. Deb, J. Chung, and N. Kjærgaard, Dispersive detection of atomic ensembles in the presence of strong lensing, New J. Phys. **22**, 073017 (2020).

[40] D. B. Hume, I. Stroescu, M. Joos, W. Muessel, H. Strobel, and M. K. Oberthaler, Accurate Atom Counting in Mesoscopic Ensembles, Phys. Rev. Lett. **111**, 253001 (2013).

[41] J. Bechhoefer, Feedback for physicists: A tutorial essay on control, Rev. Mod. Phys. **77**, 783 (2005).

[42] *IEEE Standard Definitions of Physical Quantities for Fundamental Frequency and Time Metrology-Random Instabilities* (2009).

[43] APDs experience excess noise above the photon shot noise, which is expressed as a multiplicative factor F [46]. We measure $F = 7.6$ for our APDs.

[44] J. Zeiher, J. Wolf, J. A. Isaacs, J. Kohler, and D. M. Stamper-Kurn, Tracking Evaporative Cooling of a Mesoscopic Atomic Quantum gas in Real Time, Phys. Rev. X **11**, 041017 (2021).

[45] R. Thomas, Software and hardware code for atom number stabilisation via Faraday rotation, https://github.com/kjaergaard-lab/faraday-number-stabilisation (2021).

[46] R. McIntyre, Multiplication noise in uniform avalanche diodes, IEEE Trans. Electron Devices **ED-13**, 164 (1966).